EJNMMI Physics

ORIGINAL RESEARCH Open Access

Establishing measurement traceability for quantitative SPECT imaging

Andrew P. Robinson[1*], Kelley M. Ferreira[1,2,3], Warda Heetun[1,4], Manuel Bardiès[5], Ana M. Denis-Bacelar[1], Andrew J. Fenwick[1], Michael Lassmann[6], Jill Tipping[7] and Johannes Tran-Gia[6]

*Correspondence:
andrew.robinson@npl.co.uk

[1] National Physical Laboratory, Hampton Road, London TW11 0LW, UK
[2] Department of Oncology, University of Oxford, Oxford, UK
[3] Oxford University Hospitals NHS Foundation Trust, Oxford, UK
[4] St.Georges Hospital, London, UK
[5] Cancer Research Institute of Montpellier, U1194, INSERM/ICM/Montpellier University, 208 Av des Apothicaires, 34298 Montpellier cedex 5, France
[6] Department of Nuclear Medicine, University Hospital Würzburg, Würzburg, Germany
[7] Christie Medical Physics and Engineering (CMPE), The Christie NHS Foundation Trust, Wilmslow Road, Manchester M20 4BX, UK

Abstract

Background: Single Photon Emission Computed Tomography (SPECT) is increasingly used as a quantitative modality, especially in the context of Molecular Radiotherapy, where the measurements are used as input to absorbed dose calculations for patient-specific dosimetry. Establishing measurement traceability is an essential step in providing confidence in quantitative measurements. This requires an unbroken chain of calibrations where uncertainties must be reported in all stages of calibration and for the final measurement result. Traceability ensures that a measurement result can be related to an underlying standard, allowing harmonisation of data, and facilitating comparison of results between sites.

Methods: The process of establishing measurement traceability for quantitative SPECT is demonstrated for the therapeutic radionuclide ^{177}Lu using a common, phantom based, calibration method. Phantoms with activities of ^{177}Lu, measured using a traceably calibrated radionuclide calibrator, were used to perform the calibration. The calibration was validated using 3D-printed anthropomorphic organ phantom inserts mimicking clinically relevant geometries. For all measurements, traceability to primary standards for radioactivity is demonstrated along with an accompanying calibration chain and statement of uncertainty.

Results: For all activity measurements the dominant component in the activity uncertainty budget was the uncertainty on the radionuclide calibrator calibration factor, resulting in an average combined standard uncertainty of 1.57%. The resulting uncertainty on the SPECT Image Calibration Factor was 1.6%. An optional additional correction was included in the calibration to provide volume-based partial volume correction (PVC). Measurement traceability was extended for measurands using this additional correction. The activity recovery in the organ phantoms with PVC applied was 96(7)% for both the kidney and spleen.

Conclusions: A manufacturer independent methodology for establishing measurement traceability for quantitative SPECT is demonstrated for ^{177}Lu, using a radionuclide calibrator previously calibrated against national standards. The ability to establish measurement traceability for quantitative SPECT using standard clinical equipment, and the limitations of traceability are presented.

Keywords: Traceability, SPECT, Quantitative imaging, Measurement uncertainty

Introduction

Traceability to primary standards of radioactivity for radiopharmaceuticals is a critical component in ensuring their safe and effective clinical use. Metrological traceability is defined as a *"property of a measurement result whereby the result can be related to a reference through a documented unbroken chain of calibrations, each contributing to the measurement uncertainty"* [1]. This traceability is only achieved by calibration against an appropriate measurement standard, with comprehensive documentation of the calibration chain, and with an accompanying assessment of uncertainty in the measurement result [2]. For measurements of radionuclide activity, both during radiopharmaceutical production and for clinical administration of radiopharmaceuticals, there are well established routes to provide traceability [2, 3]. National Metrology Institutes (NMIs) or a Designated Institute (DI—hereafter included in discussion of NMIs) are responsible for establishing primary standards for specific radionuclides and for extending traceability, through links with secondary laboratories, to end-users. These routes vary between countries and in the case when a country does not have a dedicated NMI then the primary standard from an NMI in another country may be recognised.

Single Photon Emission Computed Tomography (SPECT) is now increasingly being used as a quantitative modality, often coupled with x-ray CT to provide attenuation correction [4]. As such, the chain of measurement traceability should be extended to these SPECT measurements and calibrations [5]. Traceability for SPECT measurements necessitates a traceable calibration relating a measured 3D distribution of counts to a known activity of a specific radionuclide. Whilst the exact route for traceability depends on the specific calibration and measurement methodologies, all techniques require accurate traceable activity measurements, transferred to a phantom geometry (or a sealed source in the case of manufacturer supplied sources), and the careful propagation of uncertainties through any subsequent measurements and calculations. Establishing traceability ensures that a measurement result can be related to an underlying standard. This provides multiple benefits including increased confidence in the measurement results for clinical users, harmonisation of measurements across sites, and fulfilling regulatory requirements. Traceable calibration of SPECT imaging is especially important for Molecular Radiotherapy where the measurements are used as input to absorbed dose calculations for patient-specific treatment optimisation.

In this work the process of establishing measurement traceability for SPECT quantitative imaging (QI) is demonstrated for the therapeutic radionuclide ^{177}Lu using a common, phantom based, calibration method. An example of a complete traceability chain from primary standard to quantitative SPECT measurement is derived. In contrast to quantification procedures commonly provided by equipment manufacturers, using an open calibration method (which optionally may reproduce the manufacturer calibration) allows the propagation of input uncertainty components to the total calibration uncertainty, a requirement of measurement traceability. The presented methodology can be easily adapted to common SPECT calibration methodologies, allowing clinical centres to establish traceability for quantitative SPECT measurements.

Methods

A range of guidance on quantitative SPECT/CT imaging [4, 6–8] has been published and manufacturers are increasingly providing methods for QI for common radionuclides. All methods of SPECT calibration are dependent on some form of test object or phantom with known activity of a specific radionuclide. Regardless of the calibration method used, these phantoms, and the methods used in their preparation, define the traceability route for SPECT QI–provided that there is an accompanying assessment of uncertainty in the measurement result. This requires that the phantoms used for the calibration and validation of quantitative SPECT imaging systems are filled with an activity traceable to national standards [9].

In this work, measurement traceability for ^{177}Lu SPECT QI is demonstrated for a common phantom based calibration methodology [8] using three phantoms: a cylindrical Jaszczak phantom with uniform activity distribution, a NEMA IEC PET Body phantom (NEMA) [10] with 6 spherical inserts (with diameters 10–37 mm) filled with uniform activity distribution in a cold background, and two 3D-printed anthropomorphic organ phantom inserts mimicking clinically relevant geometries [8, 11]. This method calculates an Image Calibration Factor (*ICF*) to relate the detected count rate to an instantaneous radionuclide activity, derives a volume-based correction for partial volume effects (PVE) [12] and uses a realistic test object to validate the calibration. For all measurements, traceability to primary standards for radioactivity is demonstrated along with an accompanying statement of uncertainty.

Whilst large volume phantoms are commonly used to calibrate SPECT systems, alternative calibration methods using planar images of point sources, vials, line sources and petri dishes may also be used [6, 14]. The techniques for establishing traceability for the calibration method in this work can be easily adapted to other common SPECT calibration methodologies and additional radionuclides. A summary of the calibration method and measurements results, indicating the traceability route, is shown in Fig 1. Full details of the calibration method and accompanying measurements are provided in the remainder of this section.

Activity measurement

Radionuclide calibrators are widely used for the measurement of activity of radioactive solutions before administration to patients and provide the most common route for dissemination of primary activity measurements into the clinic [15, 16]. Calibration factors (or dial settings) for a radionuclide calibrator, relating the time-averaged ionisation current to the activity of the radionuclide sample, can be determined using a primary standard source. In this case, the radionuclide calibrator may be considered a secondary standard. It is important to note that calibration factors are determined for a standard volume in a particular container geometry and any deviation from this can require the determination of a new calibration factor (for example by cross calibration with a secondary standard calibrator or traceable source) to maintain measurement traceability and accuracy. Extensive guidance for the calibration of radionuclide calibrators for additional geometries and novel radionuclides can be found in [15, 17].

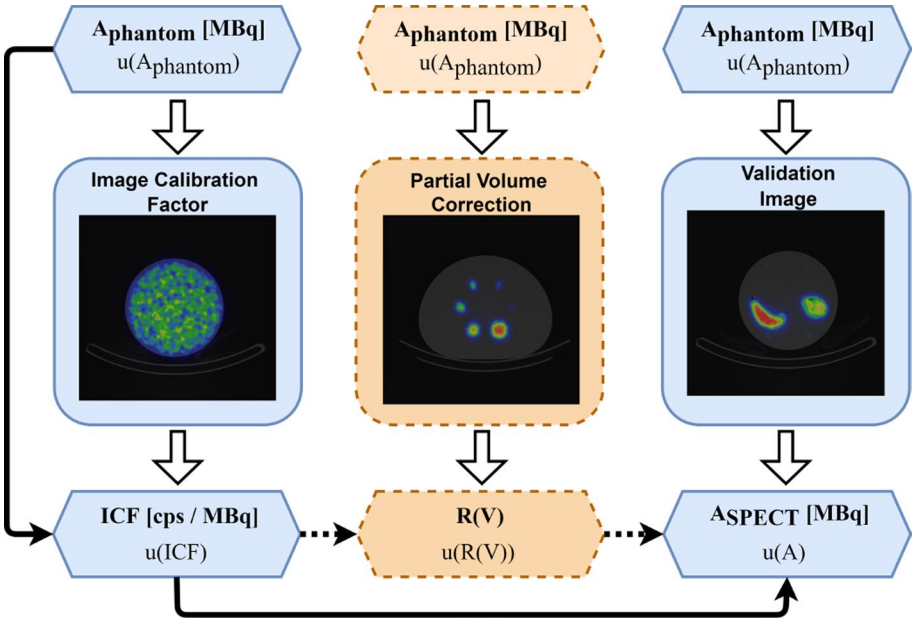

Fig. 1 Summary of measurements used in the calibration method (left: Image Calibration Factor, centre: optional partial volume correction (PVC) and right: validation measurement). Measurement results (hexagonal blocks) and SPECT/CT imaging data (rounded rectangular blocks) are indicated. A transaxial slice through the SPECT/CT data is shown for each acquisition. Black arrows indicate the traceability route for measurement results. If the PVC is applied then an alternative traceability route is required (black dashed line). Each measurement result requires both the value of the measurement result and an estimate of the uncertainty in the result [13]. Full definitions of the measurands are given in Eqs. (2), (6), (8), (15) and (20)

For this work a Capintec CRC-25R radionuclide calibrator, calibrated against the National Physical Laboratory (NPL) secondary standard ionisation chamber, was used for all activity measurements. The calibration measurement geometry for ^{177}Lu was 4 mL of solution in a ISO 8362-1-A-10R-cl-1 vial (hereinafter referred to as a 10R vial) [18]. The accuracy of this calibrator system is representative of a routinely calibrated clinical system with a robust quality control system in place.

Radionuclide calibrator measurements should be corrected for the presence of background radioactivity, determined by measuring without sources in the chamber, and decay corrected to a common reference time, t_{ref}, where appropriate. In this work all reported activities have had background and decay correction applied, according to Eq. (1) using a half-life ($t_{1/2}$) of 6.647(8) days [19] (For all measurement results quoted in this work, the number in parentheses is the numerical value of the combined standard uncertainty referred to the corresponding last digits of the quoted result).

$$A(t_{ref}) = (a_1 - b_1)e^{-\lambda(t_{ref} - t_1)} \tag{1}$$

where, a_1 is the uncorrected activity measurement made at time t_1, b_1 is the background measurement made without sources in the chamber and λ is the decay constant ($\lambda = ln(2)/t_{1/2}$).

Phantom preparation

The calibration and validation of quantitative SPECT imaging systems requires accurate activity measurements at a defined reference time, and a uniform distribution of activity within the phantom volumes. The activity in the phantom should be traceable to national primary standards of radioactivity, as highlighted in [20–22]. The different production routes of radionuclides can impact the radionuclide purity of the solution, and therefore when possible, impurity free radionuclides should be used. Suppliers of radionuclides commonly provide the solution in a glass vial and in a limited volume. Dilution of radioactive source and phantom preparation should be done using an appropriate carrier for the radionuclide of interest, to avoid the solution sticking to the walls of the containers/phantoms and to ensure homogeneous solutions. Examples of carrier solution preparation for commonly used radionuclides in nuclear medicine are presented in [9]. Multiple methods can be used to measure the total activity dispensed to a phantom, and the choice of method is user and equipment dependent. Complete guidance on how to prepare a phantom with an activity traceable to national standards using these methods can be found in [9]. These methodologies can be divided into two main categories for which, the activity in the phantom is estimated either based solely on radionuclide calibrator measurements, or based on radionuclide calibrator measurements and the use of a balance. Details of the specific methods used to prepare the phantoms in this work are provided in the following sections.

Cylindrical phantom

Approximately 4 g of ^{177}Lu chloride solution was dispensed to a 10R vial and the activity was measured on the radionuclide calibrator (A_1). A cylindrical Jaszczak phantom (corresponding to a large volume of approximately 6.9 L) was filled to 75% of its volume using a carrier solution of 0.1 mol L^{-1} HCl containing 10 $\mu g\ g^{-1}$ of inactive lutetium standard element. The solution in the 10R vial was dispensed to the phantom using a syringe. The activity in the full syringe was measured on the radionuclide calibrator using a calibration factor for 4 mL of solution in a 10R vial (A_3). The solution was then dispensed to the phantom, mixed, and the phantom was filled with carrier to its full capacity. Both the vial and syringe were refilled with 4 mL of carrier solution (to match the initial volume and geometry), and the activities measured (A_2 and A_4 respectively).

The total activity in the phantom was calculated using Eq. (2).

$$A_{ph}(t_{ref}) = \left(A_1(t_{ref}) - A_2(t_{ref})\right).\left(1 - \frac{A_4(t_{ref})}{A_3(t_{ref})}\right) \tag{2}$$

The 10R vial activities full (A_1) and residue (A_2), and the syringe full (A_3) and residue (A_4) were measured using the same radionuclide calibrator and therefore the measurements are correlated. The output of the radionuclide calibrator used in this work is in units of activity (Bq) and the measured current is not recorded. As a result, the uncertainty component due to the calibration factor (CF) in $A_{ph}(t_{ref})$ can not be calculated analytically, and the correlated uncertainty components between the activities can not be considered directly. The uncorrelated uncertainties on individual activity measurements, including background measurements ($u(a)$ and $u(b)$), were found from the standard deviation of

a set of 10 readings. The uncertainty on all time measurements in this work ($u(t)$) was assumed to be 1 sec.

The correlated calibration factor fractional uncertainty was estimated at the time of calibrating the radionuclide calibrator against national standards ($u(CF)$). A fractional uncertainty component for the reproducibility of the system was included, corresponding to the standard deviation of 75 measurements of a long-lived radionuclide over a period of time ($u(A_{repro})$). A fractional accuracy and linearity uncertainty ($u(A_{linear})$), as provided by the manufacturer of the radionuclide calibrator, was also included. The uncertainty due to the decay constant ($u(\lambda)$) is given in [19]. The combined correlated and uncorrelated uncertainties for $A_{ph}(t_{ref})$, including the background and decay correction (Eq. (1)), can therefore be estimated as:

$$\begin{aligned} u(A_{ph}(t_{ref}))^2 = \sum_{i=1}^{4} \Bigg[\left(\frac{\partial A_{ph}(t_{ref})}{\partial a_i} \right)^2 u(a_i)^2 + \left(\frac{\partial A_{ph}(t_{ref})}{\partial b_i} \right)^2 u(b_i)^2 \\ + \left(\frac{\partial A_{ph}(t_{ref})}{\partial t_i} \right)^2 u(t_i)^2 \Bigg] + \left(\frac{\partial A_{ph}(t_{ref})}{\partial \lambda} \right)^2 u(\lambda)^2 \\ + A_{ph}(t_{ref})^2 u(CF)^2 + A_{ph}(t_{ref})^2 u(A_{repro})^2 \\ + A_{ph}(t_{ref})^2 u(A_{linear})^2 \end{aligned} \tag{3}$$

NEMA spherical inserts

A stock solution of ^{177}Lu chloride was prepared at a nominal activity per unit mass of 2 MBq g^{-1}, as described in [9]. The nominal activity stock solution was then dispensed gravimetrically to a set of NEMA spheres of different diameters (10, 13, 17, 22, 28, and 37 mm) and two 10R vials, filled before (vial-1) and after (vial-2) dispensing the solution to the spheres. The spheres with activity were placed in the NEMA phantom without the lung insert, and the phantom shell was filled with deionised water. The activities of vial-1 and vial-2 were measured on the radionuclide calibrator and the activity per unit mass of the stock solution, A_m, was calculated using Eq. (4):

$$A_m(t_{ref}) = \frac{A_{vial}(t_{ref})}{m_{vial}} \tag{4}$$

where A_{vial} is the total activity measured in the vial (corrected using Eq. (1)) and m_{vial} is the total mass dispensed to the vial. The activity per unit mass of vial-1 and vial-2 were compared to assess the homogeneity of the stock solution. The standard uncertainty for the activity per unit mass ($u(A_m)$) can be expressed as:

$$\left(\frac{u(A_m(t_{ref}))}{A_m(t_{ref})} \right)^2 = \left(\frac{u(A_{vial}(t_{ref}))}{A_{vial}(t_{ref})} \right)^2 + \left(\frac{u(m_{vial})}{m_{vial}} \right)^2 \tag{5}$$

where $u(m_{vial})$ is the weighing uncertainty calculated using the accuracy of the balance assuming a rectangular probability distribution and $u(A_{vial})$ is calculated using Eq. (3) with $i = 1$. The total activity in each sphere was then calculated from A_m and the dispensed mass per spherical insert (m_{insert}):

Table 1 Acquisition parameters for the ^{177}Lu SPECT/CT data from a Mediso AnyScan SCP system

Acquisition parameters	
Collimator	Medium-Low Energy General Purpose (MLEGP)
Photopeak Energy (keV)	208.4 ± 20.8 (20% width)
Lower Scatter Energy (keV)	181.3 ± 5.4 (6% width)
High Scatter Energy (keV)	235.5 ± 7.1 (6 % width)
Matrix size	128 x 128
Pixel size (mm)	4.2578
SPECT movement	Body Contour
Number of projections	120
Time per projection	60 s
Detector movement	Step and Shoot
CT	Low Dose (80 kVp, 50 mAs)

Table 2 Reconstruction parameters for the ^{177}Lu SPECT/CT data from a Mediso AnyScan SCP system

Reconstruction parameters	
Attenuation Correction	CT based
Scatter Correction	Triple Energy (TEW)
Iterations	25
Matrix size	128 x 128
Pixel size (mm)	4.2578
Subsets	2
Post-filter	None
Resolution recovery	None

$$A_{sphere}(t_{ref}) = A_m(t_{ref}).m_{insert} \tag{6}$$

The corresponding standard uncertainty, $u(A_{sphere})$, is given by:

$$\left(\frac{u(A_{sphere}(t_{ref}))}{A_{sphere}}\right)^2 = \left(\frac{u(A_m(t_{ref}))}{A_m(t_{ref})}\right)^2 + \left(\frac{u(m_{insert})}{m_{insert}}\right)^2 \tag{7}$$

Validation phantom

To prepare the 3D-printed phantom inserts [8, 11] a stock solution at a nominal activity per unit mass of 20 MBq g^{-1} was prepared following the guidance in [9]. Activity was dispensed gravimetrically to the three phantom insert compartments, with inactive carrier solution (as previously described) added to fill the insert volumes. The total activity in the inserts was calculated using the activity per unit mass (MBq g^{-1}) and the mass of radioactive solution dispensed to the inserts. The organ inserts were then fully rotated 10 times to ensure full mixing.

SPECT activity calibration

SPECT/CT data was acquired on a Mediso AnyScan SCP system for the three phantoms described in the previous section, using the acquisition parameters described in Table 1.

The start time of each scan was recorded using a time signal traceable to national standards. A common set of reconstruction parameters was used to process all data sets with the manufacturer supplied software (using Ordered Subset Expectation Maximization (OS-EM)), with an external Triple Energy Window (TEW) scatter correction applied), as described in Table 2.

Image calibration factor

The SPECT/CT data for the cylindrical Jaszczak phantom was used to determine an Image Calibration Factor (*ICF*) relating the counts per second (cps) in a reconstructed image to the dispensed activity (in Bq):

$$ICF = \frac{C_{ph}}{T_{ph} \cdot A_{ph}(t_{ref})} \tag{8}$$

where C_{ph} is the counts in the reconstructed image within a cylindrical volume of interest (VOI) corresponding to 130% of the radius and 120% of the height of the phantom [8]; T_{ph} is the SPECT acquisition duration (in seconds); and A_{ph} is the total activity dispensed in the phantom measured using a radionuclide calibrator, decay corrected to the start of the SPECT acquisition (Eq. (2)). The combined uncertainty associated with *ICF* ($u(ICF)$) can be expressed as shown in Eq. (9):

$$\left(\frac{u(ICF)}{ICF}\right)^2 = \left(\frac{u(C_{ph})}{C_{ph}}\right)^2 + \left(\frac{u(T_{ph})}{T_{ph}}\right)^2 + \left(\frac{u(A_{ph}(t_{ref}))}{A_{ph}(t_{ref})}\right)^2 \tag{9}$$

where $u(C_{ph})$ is the standard uncertainty in C_{ph}, $u(T_{ph})$ is the standard uncertainty in T_{ph} and $u(A_{ph})$ is the standard uncertainty in the activity dispensed to the phantom (Eq. (3)).

It has been well established that, whilst raw data and the position and energy estimates constructing a SPECT sinogram may be modelled as a Poisson random variable [23], the resulting reconstructed image may not strictly be modelled by a Poisson distribution [24]. A rigorous assessment of the uncertainty associated with a measurement of counts in an iteratively reconstructed SPECT image is both outside of the scope of this work and any current practical feasibility with a clinical SPECT/CT system. In this work we estimate this uncertainty using a Poisson distribution, with the caveat that this approximation may underestimate the magnitude of this component (as an example, a factor of ~4 is seen in [25]).

$$u(C_{ph}) = \sqrt{C_{ph}} \tag{10}$$

There are a number of considerations which should be made when applying this approximation. Care should be taken to check for arbitrary normalisation or scaling factors that may be introduced within the reconstruction algorithm, inflating the number of reconstructed counts compared to the acquired sinogram, resulting in an underestimation of uncertainty. If this factor can not be removed then the effect can be partially compensated for by considering the fractional Poisson uncertainty in the VOI based on the acquired sinogram statistics. When considering quantification of smaller VOIs, which typically contain lower counts, the impact of the count uncertainty underestimation may become more significant. In general, the relative contribution of counts uncertainty

to the total uncertainty of any measurement should be assessed to determine if a more complete treatment of this uncertainty component is required.

Partial volume correction

To correct for partial volume effects an approach based on measurements of activity recovery for a range of known volumes is applied to compensate for spill-out from a VOI. It should be noted that the application of partial volume correction is not explicitly required for traceable quantitative SPECT imaging, but is included as an example of how to ensure traceability when additional corrections are applied. Furthermore, establishing traceability does not guarantee the accuracy of the correction method, which has been shown to vary depending on the target geometry [26, 27]. An activity recovery curve was determined based on the NEMA phantom with spheres of different sizes. VOIs were drawn on the CT images for the 6 spheres, corresponding to the known inner diameter of the spheres. The recovery coefficients of each sphere insert (R_{sphere}) were calculated as the ratio between the activities from the calibrated SPECT imaging and the radionuclide calibrator measurement:

$$R_{sphere} = \frac{A_{sphere}^{SPECT}}{A_{sphere}} \tag{11}$$

where A_{sphere} is the activity in a spherical insert determined using a radionuclide calibrator traceable to national standards (Eq. (6)) and A_{sphere}^{SPECT} is defined in Eq. (12).

$$A_{sphere}^{SPECT} = \frac{C_{sphere}}{T_{sphere}.ICF} \tag{12}$$

where, C_{sphere} is the measured counts in the VOI for each sphere in the reconstructed image; T_{sphere} is the total acquisition duration, and ICF is the image calibration factor calculated using Eq. (8). The uncertainty in A_{sphere}^{SPECT} was calculated using Eq. (13):

$$\left(\frac{u(A_{sphere}^{SPECT})}{A_{sphere}^{SPECT}}\right)^2 = \left(\frac{u(C_{sphere})}{C_{sphere}}\right)^2 + \left(\frac{u(T_{sphere})}{T_{sphere}}\right)^2 + \left(\frac{u(ICF)}{ICF}\right)^2 \tag{13}$$

where $u(C_{sphere})$ is the standard uncertainty in C_{sphere} (from Eq. (10)) and $u(ICF)$ is given by Eq. (9).

The uncertainty on the recovery coefficient (Eq. (14)) (R_{sphere}) can be found using Eqs. (3), (7), (9) and (13), with a_{1-4}, b_{1-4} and t_{1-4} as defined in Eq. (3) and a_5, b_5 and t_5 being the values associated with the measurement of $A_{vial}(t_{ref})$ in Eq. (4), with a single set of the correlated uncertainties:

$$
\begin{aligned}
u(R_{sphere})^2 = \sum_{i=1}^{5} \Bigg[& \left(\frac{\partial R_{sphere}}{\partial a_i} \right)^2 u(a_i)^2 + \left(\frac{\partial R_{sphere}}{\partial b_i} \right)^2 u(b_i)^2 \\
& + \left(\frac{\partial R_{sphere}}{\partial t_i} \right)^2 u(t_i)^2 \Bigg] + \left(\frac{\partial R_{sphere}}{\partial \lambda} \right)^2 u(\lambda)^2 \\
& + R_{sphere}^2 u(CF)^2 + R_{sphere}^2 u(A_{repro})^2 + R_{sphere}^2 u(A_{linear})^2 \\
& + \left(\frac{\partial R_{sphere}}{\partial C_{sphere}} \right)^2 u(C_{sphere})^2 + \left(\frac{\partial R_{sphere}}{\partial C_{ph}} \right)^2 u(C_{ph})^2 \\
& + \left(\frac{\partial R_{sphere}}{\partial T_{sphere}} \right)^2 u(T_{sphere})^2 + \left(\frac{\partial R_{sphere}}{\partial T_{ph}} \right)^2 u(T_{ph})^2
\end{aligned} \tag{14}
$$

A volume dependent recovery coefficient curve was found by fitting a two-parameter model [8], shown in Eq. (15), to the calculated recovery coefficients (Eq. (11)), using a weighted nonlinear regression model (Levenberg-Marquardt algorithm in MATLAB 2020a [28, 29]). The weight (W_i) of the points used in the fit can be calculated using Eq. (16) and can be adjusted for the uncertainty in the volumes, to account for the difficulty of estimating recovery coefficients for smaller volumes.

$$
R(V) = \frac{1}{1 + (\frac{\alpha}{V})^{\beta}} \tag{15}
$$

$$
W_{sphere} = \frac{RC_{sphere}}{u(RC_{sphere})} \times \frac{V_{sphere}}{u(V_{sphere})} \tag{16}
$$

The uncertainty associated with the fitted recovery for a given volume, $RC(V)$, can be estimated as shown in Eq. (17):

$$
u(R(V))^2 = \left(\frac{\partial(R)}{\partial \alpha} \right)^2 u(\alpha)^2 + \left(\frac{\partial(R)}{\partial \beta} \right)^2 u(\beta)^2 + \left(\frac{\partial(R)}{\partial(V)} \right)^2 u(V)^2 \tag{17}
$$

where $u(\alpha)$ and $u(\beta)$ are the uncertainties in the values of the parameters from the weighted nonlinear regression model. The uncertainty for a measured volume was estimated [30] as shown in Eqs. (18) and (19), assuming a sphere of diameter, d_{sphere} and a SPECT voxel size, a, of 4.4 mm with FWHM of 15 mm.

$$
u(d_{sphere})^2 = \frac{a^2}{6} + \frac{FWHM^2}{4ln2} \tag{18}
$$

$$
\left(\frac{u(V_{sphere})}{u(V_{sphere})} \right)^2 = \left(3 \frac{u(d_{sphere})}{d_{sphere}} \right)^2 \tag{19}
$$

Calibration validation

The final stage of the SPECT calibration is to validate the calibration result, providing an independent check of the activity quantification from SPECT images. This can be done by scanning an additional phantom with a known and traceable activity. The validation data must be reconstructed using the same reconstruction parameters used

to reconstruct the activity calibration data. In this work 3D-printed anthropomorphic organ phantom inserts [8, 11] (as previously described) are used for the validation. The VOIs for the 3D-printed inserts were outlined on the CT images where the inserts were clearly delineated. Consequently, no additional uncertainties relating to the choice of VOI were considered. In addition, the uncertainty due to the algorithm used to assign counts to the VOI was not considered.

As previously discussed, activity recovery coefficients and standard uncertainty for the validation phantom can be calculated from Eqs. (11) and (14), applying the same treatment to the estimation of correlated measurement uncertainties. The SPECT activity in the validation phantom organ inserts with PVC applied can be calculated using Eq. (20):

$$A_{SPECT}(V_{organ}) = \frac{C_{organ}}{T_{organ}.ICF.R(V_{organ})} \tag{20}$$

where, C_{organ} is the measured counts in the reconstructed image within the volume of interest, V_{organ}; the recovery factor, $R(V_{organ})$, can be estimated using Eq. (15); T_{organ} is the total acquisition duration (in sec) and ICF is the image calibration factor calculated using Eq. (8). The uncertainty on the SPECT activity, $u(A_{SPECT}(V_{organ}))$, in a validation phantom organ insert can be estimated using Eq. (21):

$$\begin{aligned}\left(\frac{u(A_{SPECT}(V_p))}{A_{SPECT}(V_p)}\right)^2 =& \left(\frac{u(C_{organ})}{C_{organ}}\right)^2 + \left(\frac{u(T_{organ})}{T_{organ}}\right)^2 \\ &+ \left(\frac{u(ICF)}{ICF}\right)^2 + \left(\frac{u(R(V_{organ}))}{R(V_{organ})}\right)^2\end{aligned} \tag{21}$$

Results

Phantom preparation

Cylindrical phantom

Radionuclide calibrator activity measurements from filling the cylindrical phantom are reported in Table 3. The dispensed activity values are reported with background correction applied and decay corrected to the SPECT imaging reference time (27/03/2019 16:32 UTC).

The total activity (A_{ph}) dispensed to the cylindrical phantom (Eq. (2)) was 410.1(66) MBq. The combined uncertainty budget for A_{ph} is given in Table 4, including the standard deviation from repeated measurements of the sources (N = 10) and the uncertainty from the decay correction.

Table 3 Activity measurements for preparation of cylindrical phantom

	Activity (MBq)
A_1	431.1(67)
A_2	11.30(17)
A_3	440.4(68)
A_4	10.23(16)

Data is background corrected and decay corrected to SPECT imaging reference time

Table 4 Uncertainty budget for total activity in cylindrical phantom (standard uncertainties at $k = 1$)

Component	Uncertainty (%)
Calibration Factor (*CF*)	1.0
Reproducibility (A_{repro})	0.5
Linearity (A_{linear})	1.0
Background (b_1)	0.31
Background (b_2)	0.30
Background (b_3)	4.1×10^{-7}
Background (b_4)	7.8×10^{-3}
Activity (a_1)	0.13
Activity (a_2)	0.14
Activity (a_3)	1.3×10^{-7}
Activity (a_4)	0.012
λ	0.37
t_1	0.060
t_2	0.0015
t_3	3.5×10^{-5}
t_4	7.9×10^{-7}
t_{ref}	0.046
Combined uncertainty (u_c)	**1.62**

Table 5 Total mass and corresponding activities dispensed to vial-1 and vial-2 (10R Schott vials)

Description	vial-1	vial-2
Vial empty (g)	11.2198(1)	11.1892(1)
Vial full (g)	15.2105(1)	15.2242(1)
Total mass (g)	3.9947(2)	4.039(2)
Activity (MBq)	8.60(13)	8.67(13)
Activity per unit mass (MBq g^{-1})	2.152(33)	2.147(33)

The activity per unit mass of the stock solution is also reported at the SPECT imaging reference time

Table 6 Uncertainty budget for total activity per unit mass (MBq g^{-1}) of the stock solution used to prepare the spherical inserts (standard uncertainties at $k = 1$)

Component	Uncertainty (%)
Calibration Factor (*CF*)	1.0
Activity (a_1)	0.15
Reproducibility (A_{repro})	0.5
Background (b_1)	0.32
Linearity (A_{linear})	1.0
λ	0.027
t_1	0.0037
Weighing (m_{vial})	0.025
Combined uncertainty (u_c)	**1.54**

NEMA spherical inserts

The total mass dispensed, measured activities, and activity per unit mass, for the two 10R vials (vial-1 and vial-2) are presented in Table 5. The uncertainty budget for the total activity

Table 7 Mass and total activity dispensed to spherical inserts, reported at the SPECT imaging reference time

Sphere diameter Nominal (mm)	Dispensed mass (g)	Total activity (MBq)
10	0.5347(1)	1.151(18)
13	1.1658(1)	2.509(39)
17	2.6338(1)	5.668(87)
22	5.6292(1)	12.11(19)
28	11.5140(1)	24.78(38)
37	27.9753(1)	60.20(93)

Table 8 Mass of radioactive solution, total mass and total activity in the 3D-printed organ inserts at SPECT imaging reference time

Insert	Radioactive solution mass (g)	Total mass (g)	Total activity (MBq)
Kidney–medulla	1.0943(2)	34.0406(22)	22.33(35)
Kidney–cortex	5.3510(2)	74.8157(21)	109.2(17)
Kidney–total	6.4453(2)	108.8563(78)	131.5(21)
Spleen	8.8758(2)	124.2964(69)	181.2(28)

Table 9 Components used to calculate the ICF

Component	Value
Counts (arb)	20879094(5857)
Total Acquisition Duration (s)	3600(1)
A_{ph} (MBq)	410.1(66)
ICF (cps/MBq)	**14.14(23)**

A_{ph} is decay corrected to the SPECT acquisition time

per unit mass (MBq g^{-1}) of the vials is shown in Table 6. The activity per unit mass in vial-1 and vial-2 was in statistical agreement suggesting the solution was homogeneous, therefore values from vial-1 were used for further calculations.

The activity per unit mass of the solution dispensed to the spherical inserts was 2.152(33) MBq g^{-1} at 28/03/2019 16:52 UTC. The dispensed mass of radioactive solution, and total activity dispensed to the spherical inserts is reported in Table 7.

Validation phantom

The mass of radioactive solution, total mass and total activity dispensed to the 3D-printed organs are reported in Table 8, from a stock solution with an activity per unit mass of 20.41(32) MBq g^{-1} at 29/03/2019 17:00 UTC.

Table 10 Activity in the spherical inserts decay corrected to the SPECT acquisition time

Sphere diameter Nominal (mm)	Activity (MBq)	Total counts (Counts)	A_{sphere}^{SPECT} (MBq)	R_{sphere}
10	1.151(18)	6031(116)	0.1185(30)	0.1029(26)
13	2.509(39)	31970(267)	0.628(11)	0.2503(46)
17	5.668(87)	90440(449)	1.777(30)	0.3135(54)
22	12.11(19)	218439(697)	4.291(71)	0.3544(60)
28	24.78(38)	522957(1079)	10.27(17)	0.4146(69)
37	60.20(93)	1514023(1836)	29.74(48)	0.4941(82)

Total counts in the VOI in the reconstructed SPECT and activity measured in the reconstructed SPECT data calculated using Eq. (12). Activity recovery factors for the spherical inserts are also shown

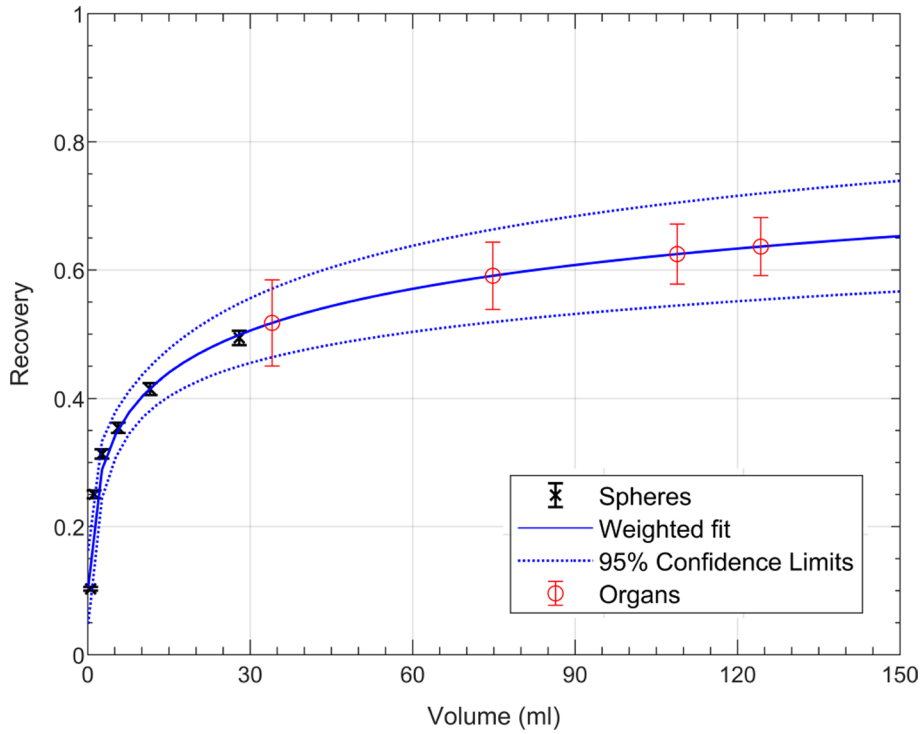

Fig. 2 Recovery curve for the NEMA spheres fitted using Eq. (15). The reported uncertainties (dashed lines) are expanded uncertainties at a confidence level of 95%. The calculated recovery coefficients for the 3D-printed inserts (organs) from the fitted data are presented in red with the corresponding uncertainties. The weighted fit to the data (solid blue line) is shown

SPECT activity calibration

Image calibration factor

The total counts in the reconstructed SPECT imaging and total acquisition duration used to calculate the *ICF* (Eq. (8)) are reported in Table 9. The calculated *ICF* was 14.14(23) cps/MBq. It should be noted that the calculated *ICF* is reconstruction and equipment specific. The uncertainty on the acquisition duration was assumed to be 1 s at $k = 1$, the uncertainty in the total counts was estimated using Eq. (10), and the uncertainty in the phantom activity is given in Table 4.

Table 11 Calculated recovery factors ($R(V_{organ})$) for the 3D-printed organ inserts

Insert	$R(V_{organ})$
Kidney–medulla	0.517(67)
Kidney–cortex	0.591(52)
Kidney–total	0.625(47)
Spleen	0.637(45)

Table 12 Dispensed activity in the 3D-printed insert organs decay corrected to the SPECT acquisition time and total counts in the VOI in the reconstructed SPECT image

Insert	A_{organ} (MBq)	Counts	A^{SPECT}_{organ} (MBq) No PVC	$A^{SPECT}_{organ}/A_{organ}$	A^{SPECT}_{organ} (MBq) With PVC	$A^{SPECT}_{organ}/A_{organ}$
Medulla	22.33(35)	1519552(2309)	29.85(48)	1.34(22)	57.7(77)	2.58(34)
Cortex	109.2(17)	2508491(2967)	49.28(80)	0.4513(76)	83.4(75)	0.77(7)
Kidney	131.5(21)	4028043(3759)	79.1(13)	0.60(10)	126.6(49)	0.96(7)
Spleen	181.2(28)	5611396(4437)	110.2(18)	0.61(10)	173.2(13)	0.96(7)

Activity measured from the reconstructed SPECT data calculated using Eq. (20) and activity recovery ratios are shown with and without partial volume correction (PVC) applied

Partial volume correction

The dispensed activity in the spherical inserts, decay corrected to the SPECT imaging time, are reported in Table 10. Measured counts in the VOIs, calculated SPECT activities in the spheres, and activity recovery factors for each sphere, Eq. (11), are also presented. This data was fitted to Eq. (15) to determine the recovery curve ($\alpha = 28.3(53)$, $\beta = 0.38(5)$) and the corresponding recovery curve is presented in Fig 2.

Validation of quantitative imaging

Calculated recovery factors ($R(V_{organ})$) for the organ inserts are presented in Table 11. These values were used to apply PVC to the activity measured with SPECT imaging for each organ insert. The ratio ($A^{SPECT}_{organ}/A_{organ}$) is presented, with and without PVC, for the kidney, kidney–medulla, kidney–cortex, and the spleen in Table 12.

Discussion

In this work a detailed example of establishing traceability for quantitative ^{177}Lu SPECT/CT imaging using a phantom based calibration has been presented. A variety of techniques have been used to prepare phantoms with activities traceable to national standards, with an average uncertainty of 1.57%. In all cases the dominant component in the activity uncertainty budget was the uncertainty on the radionuclide calibrator calibration factor (CF). This result reflects the accuracy that is readily achievable in a clinical setting if appropriate guidance is followed [9, 15].

The calibration of the quantitative SPECT imaging was validated for any potential bias or uncorrected errors using an independent phantom (containing clinically representative kidney and spleen inserts). An optional additional correction was included in the calibration to provide volume-based PVC. By ensuring that the activities used to

acquire the data used as input to this correction are traceable, and that uncertainties are propagated into quantitative measurements using the correction, then traceability can be established for measurements utilising this correction. It is important to note that the inclusion or absence of a specific PVC methodology does not define the traceability of a quantitative SPECT measurement, however if a PVC correction is applied then an uncertainty budget must be established to ensure traceability. Alternative approaches to reconstruction and VOI definition have reported increased activity recovery (without additional PVC) [8, 31], however these approaches still require the establishment of an uncertainty budget.

The increased confidence and trust that comes from reporting standard uncertainties (the internationally expected standard for scientific research) for quantitative SPECT measurements is clearly demonstrated in the data presented in this work. In the case of the validation phantom organ inserts, the low activity recovery for CT-based VOIs (kidney = 0.60(10), spleen = 0.61(10)) shows that an additional correction is required to fully recover the activity in the insert. Without a corresponding uncertainty on these values, and a traceable calibration allowing the values from different phantoms to be compared, there is no a posteriori argument that the reduced recovery requires further correction (despite being lower than expected ratio of 1.0). Furthermore, when PVC is applied (to correct for the "spill out" from the inserts VOIs due to finite resolution of the scanner) the uncertainty for the corrected activity ratios allows the confidence in the measurements for whole organs (kidney = 0.96(7), spleen = 0.96(7)) to be assessed. The approximation of these organs as a sphere of equivalent volume when calculating the PVC does not appear to introduce any appreciable error, with activity ratio values within standard uncertainty of unity. It is clear however, that additional partial volume corrections are required for the multi compartment model (medulla = 2.58(34), cortex = 0.77(7)) where "spill in" from cortex into the medulla has not been corrected for.

Manufacturer-specific and alternative methods of establishing traceability

Considering the current lack of harmonisation of SPECT/CT systems in general, any form of traceability would already represent a significant step in the right direction. However, it should be emphasised that for measurement traceability to be established for a quantitative SPECT measurement, it is not sufficient to simply use a source of activity that is traceable to a national standard. Without a documented uncertainty budget, ideally incorporating all known sources of uncertainty, and a documented calibration chain from the quantitative measurand to the underlying standard, a quantitative SPECT measurement can not be considered traceable.

In this work an independent method of calibrating the response of a SPECT system has been used [8]. The open nature of this method allows uncertainties to be propagated through the calculation to establish traceability for measurands. To our knowledge, no manufacturer supplied calibration method for quantitative SPECT provides an uncertainty estimate for the calibration or any subsequent measurements. If the details of the calibration method are unavailable for an independent uncertainty evaluation, claims of traceability are inappropriate. Similarly, the use of a traceable source within a calibration of a system does not inherently bestow traceability to measurements made with the system.

Alternative methods of activity measurement, such as using a High Purity Germanium (HPGe) detector calibrated for the radionuclide of interest in an appropriate geometry) may also be used to provide traceability with a comparable uncertainty. In the case where a source is supplied with an accompanying calibration certificate then this value may be used to establish traceability providing the calibration and uncertainty budget are appropriately documented. However if a source is supplied with large activity uncertainties or with no documented traceability this may require independent measurement before traceability can be adequately established.

Clinical implications and practical challenges of traceability

Measurement traceability provides the foundation for meaningful comparison of quantitative SPECT results across different systems and institutions. While establishing traceability does not eliminate potential sources of error or guarantee sufficiently small measurement uncertainties for clinical use, it ensures that results are linked to an appropriate standard with a documented uncertainty. This forms the basis for optimising measurements, reducing uncertainty, and enabling further inter-site comparisons, as demonstrated in [8].

The adoption of traceability in nuclear medicine imaging has significant potential to improve the trustworthiness of results, particularly for diagnostic and therapeutic applications. For example, in molecular radiotherapy dosimetry workflows, measurement uncertainty directly impacts the accuracy of absorbed dose estimates. By establishing traceability, absorbed dose measurements can be reliably compared across clinical sites, enabling improved data collection and treatment outcomes. This work provides a comprehensive approach to uncertainty calculation for a specific dosimetry workflow, however without the inclusion of underpinning traceability routes for activity measurements, and for the nuclear data used in the absorbed dose calculation, traceability can not be established.

As previously discussed, if the measurand for which traceability is being established is related to a small VOI (or VOI with low total counts) then the approximation for counts uncertainty (Eq. (10)) may be less valid. As an example, in this work for the smallest 10 mm radius sphere $u(counts)$ is the dominate component of $u(A^{SPECT}_{sphere})$ (Table 7) and so any underestimation of $u(counts)$ will be significant. It should be noted that for all other measurands in this work an arbitrary factor of 10 increase in the value of $u(counts)$ results in an average increase in combined uncertainty of just 0.4 %. As such, the treatment of this uncertainty component is appropriate to establish the traceability of the measurement result to a defined standard.

Whilst this work has set out a clear methodology for establishing traceability in SPECT QI, there remain practical challenges for routine clinical adoption. Current manufacturers' SPECT QI options do not typically include traceability or uncertainty estimates, requiring independent validation and additional calculations. For clinical measurements to be traceable, the uncertainties must be appropriately estimated and documented. Furthermore, any software used for these calculations must comply with regulatory requirements, particularly if the data are to influence patient management.

In this work, we have demonstrated that measurement traceability can be established using standard clinical equipment. By incorporating the dominant uncertainty

components into the uncertainty budget, a pragmatic approach to handling correlated uncertainties in clinical radionuclide calibrators can be applied. This methodology can be easily expanded to include all routinely used radionuclides, provided an appropriate primary standard for activity exists as the basis of traceability. Importantly, establishing traceability in this way enables the harmonised collection of data, e.g. the absorbed dose verification following molecular radiotherapy, within multicentre efforts. Such efforts are crucial for generating the reliable data sets needed to establish absorbed dose-effect relationships in molecular radiotherapy, thus ultimately improving treatment accuracy, patient outcomes, and regulatory compliance.

Conclusion

Traceable calibration of SPECT systems is a crucial step for QI in nuclear medicine. Establishing traceability has the potential to provide confidence in QI measurements, allows inter-comparison between sites, and can harmonise measurements across sites. In this work, detailed guidance is provided for the calibration of a SPECT system for ^{177}Lu, using a radionuclide calibrator previously calibrated against national standards. The methodology presented in this work is manufacturer independent and can be applied to QI with using any SPECT system. The ability to establish measurement traceability using standard clinical equipment has been demonstrated, and this process could be easily expanded to include all routinely used radionuclides.

Author contributions

APR contributed to the data analysis, manuscript preparation and project funding. KMF and WH contributed to the data acquisitions, data analysis and manuscript preparation. AMDB contributed to the data analysis and manuscript preparation. AJF, MB, ML, JT and JTG contributed to the manuscript preparation. All authors contributed to the design of the experiment.

Funding

This project (19SIP01 PINICAL-MRT) has received funding from the EMPIR programme co-financed by the Participating States and from the European Union's Horizon 2020 research and innovation programme and from the UK National Physical Laboratory (NPL) through the National Measurement System Programmes Unit of the UK's Department of Business, Energy and Industrial Strategy.

Availability of data and materials

The datasets analysed during the current study are available from the corresponding author on reasonable request.

Declarations

Competing interests

M. Lassmann has received institutional grants from Ipsen, Nordic Nanovector, Novartis and PentixaPharm.

Received: 22 July 2024 Accepted: 4 June 2025
Published online: 23 June 2025

References

1. BIPM, IEC, IFCC, ILAC, ISO, IUPAC, IUPAP, OIML: International Vocabulary of Metrology— Basic and general concepts and associated terms (VIM). Joint Committee for Guides in Metrology, JCGM 200. 3rd ed. 2012. https://doi.org/10.59161/JCGM200-2012.
2. Karam LR. Measurement traceability in medical physics. J Med Phys. 2014;39(1):1. https://doi.org/10.4103/0971-6203.125470.
3. Zimmerman BE, Judge S. Traceability in nuclear medicine. Metrologia. 2007;44(4):127. https://doi.org/10.1088/0026-1394/44/4/S16.
4. Dickson JC, Armstrong IS, Gabiña PM, Denis-Bacelar AM, Krizsan AK, Gear JM, Van den Wyngaert T, de Geus-Oei L-F, Herrmann K. EANM practice guideline for quantitative SPECT-CT. Eur J of Nucl Med Mol Imaging. 2023;50(4):980–95. https://doi.org/10.1007/s00259-022-06028-9.
5. Fenwick AJ, Wevrett JL, Ferreira KM, Denis-Bacelar AM, Robinson AP. Quantitative imaging, dosimetry and metrology; Where do National Metrology Institutes fit in? Appl Radiat Isotopes. 2017. https://doi.org/10.1016/j.apradiso.2017.11.014.

6. Dewaraja YK, Frey EC, Sgouros G, Brill AB, Roberson P, Zanzonico PB, Ljungberg M. MIRD pamphlet No. 23: quantitative SPECT for patient-specific 3-dimensional dosimetry in internal radionuclide therapy. J Nucl Med. 2012;53(8):1310–25. https://doi.org/10.2967/jnumed.111.100123.
7. Ljungberg M. Absolute quantitation of SPECT studies. Semin Nucl Med. 2018;48(4):348–58. https://doi.org/10.1053/j.semnuclmed.2018.02.009.
8. Tran-Gia J, et al. A multicentre and multi-national evaluation of the accuracy of quantitative Lu-177 SPECT/CT imaging performed within the MRTDosimetry project. EJNMMI Phys. 2021;8(1):55. https://doi.org/10.1186/s40658-021-00397-0.
9. Ferreira KM, Bardiès M, Denis-Bacelar AM, Fenwick AJ, Heetun W, Lassmann M, Tipping J, Tran-Gia J, Robinson AP. NPL GPG 154: preparation of radioactive phantoms with an activity traceable to national standards. 2024. https://doi.org/10.47120/npl.mgpg154.
10. NEMA: National Electrical Manufacturers Association Standards Publication NU 2-2007, Performance Measurements of Positron Emission Tomographs 2007.
11. Robinson AP, Calvert N, Tipping J, Denis-Bacelar AM, Ferreira KM, Lassmann M, Tran-Gia J. Development of a validation imaging dataset for molecular radiotherapy dosimetry multicenter intercomparison exercises based on anthropomorphic phantoms. Physica Med. 2023;109:102583. https://doi.org/10.1016/j.ejmp.2023.102583.
12. Erlandsson K, Buvat I, Pretorius PH, Thomas BA, Hutton BF. A review of partial volume correction techniques for emission tomography and their applications in neurology, cardiology and oncology. Phys Med Biol. 2012;57(21):119–59. https://doi.org/10.1088/0031-9155/57/21/R119.
13. BIPM, IEC, IFCC, ILAC, ISO, IUPAC, IUPAP, OIML: Evaluation of measurement data—Guide to the expression of uncertainty in measurement. Joint Committee for Guides in Metrology, JCGM 100. 2008. https://doi.org/10.59161/JCGM100-2008F.
14. Zhao W, Esquinas PL, Hou X, Uribe CF, Gonzalez M, Beauregard J-M, Dewaraja YK, Celler A. Determination of gamma camera calibration factors for quantitation of therapeutic radioisotopes. EJNMMI Phys. 2018;5(1):8. https://doi.org/10.1186/s40658-018-0208-9.
15. Gadd R, Baker M, Nijran KS, Owens S, Thomas W, Woods MJ, Zananiri F. NPL GPG 93: protocol for establishing and maintaining the calibration of medical radionuclide calibrators and their quality control. 2006. https://eprintspublications.npl.co.uk/3661/.
16. Nickoloff E, Strauss K, Austin B, Balter S, Clarke G, Lin P-JP, McKetty M, Pina M, Rauch P, Tkacik M, Whiting J, Glasser H, Double C. The selection, use, calibration, and quality assurance of radionuclide calibrators used in nuclear medicine. Technical report, AAPM; 2012. https://doi.org/10.37206/137.
17. Holm S, Gear J, Minguez Gabina P, Ferreira K, Denis Bacelar A, Armstrong I, MacLean J, Wendorf C, Deroose CM, Zwane-Allen P, Roldao Pereira L, Kalle P, Fragoso Costa P. Radionuclide therapy management. Eur Assoc Nucl Med, Vienna. 2022. https://doi.org/10.52717/CUUN1001.
18. ISO: ISO 8362-1:2018(E); Injection containers and accessories, Part 1: Injection vials made of glass tubing. ISO. Issue: 8362-1:2018(E) Reference Number: ISO 8362-1:2018(E). 2018.
19. Bé M-M, Chisté V, Dulieu C, Browne E, Chechev V, Kuzmenko N, Helmer R, Nichols A, Schönfeld E, Dersch R. Table of radionuclides Vol. 2. Monographie BIPM-5 **2**. 2004.
20. Ferreira KM, Fenwick AJ. (123)I intercomparison exercises: assessment of measurement capabilities in UK hospitals. Appl Radiat Isot. 2018;134:108–11. https://doi.org/10.1016/j.apradiso.2017.11.015.
21. Bailey DL, Hofman MS, Forwood NJ, O'Keefe GJ, Scott AM, van Wyngaardt WM, Howe B, Kovacev O, Francis RJ. ARTnet, the ProPSMA trial investigators: accuracy of dose calibrators for 68ga pet imaging: unexpected findings in a multicenter clinical pretrial assessment. J Nucl Med. 2018;59(4):636–8. https://doi.org/10.2967/jnumed.117.202861.
22. Saldarriaga Vargas C, Bauwens M, Pooters IN, Pommé S, Peters SM, Segbers M, Jentzen W, Vogg A, van Velden FH, Meyer Viol SL, Gotthardt M. An international multi-center investigation on the accuracy of radionuclide calibrators in nuclear medicine theragnostics. EJNMMI Phys. 2020;7(69):1–18. https://doi.org/10.1186/s40658-020-00338-3.
23. Barrett Harrison H, Myers Kyle J. Foundations of Image Science. Hoboken: Wiley; 2003.
24. Barrett HH, Wilson DW, Tsui BMW. Noise properties of the EM algorithm. I. Theory. Phys Med Biol. 1994;39(5):833. https://doi.org/10.1088/0031-9155/39/5/004.
25. Teymurazyan A, Riauka T, Jans H-S, Robinson D. Properties of noise in positron emission tomography images reconstructed with filtered-backprojection and row-action maximum likelihood algorithm. J Digit Imaging. 2013;26(3):447–56. https://doi.org/10.1007/s10278-012-9511-5.
26. Gillen R, Erlandsson K, Denis-Bacelar AM, Thielemans K, Hutton BF, McQuaid SJ. Towards accurate partial volume correction in 99mTc oncology SPECT: perturbation for case-specific resolution estimation. EJNMMI Phys. 2022;9(1):59. https://doi.org/10.1186/s40658-022-00489-5.
27. De Nijs R. A novel model-based equation for size dependent mean recovery coefficients for spheres and other shapes. Physica Med. 2023;116:103174. https://doi.org/10.1016/j.ejmp.2023.103174.
28. Levenberg K. A method for the solution of certain non-linear problems in least squares. Quart Appl Math. 1944;2:164–8. https://doi.org/10.1090/qam/10666.
29. Marquardt DW. An algorithm for least-squares estimation of nonlinear parameters. J Soc Ind Appl Math. 1963;11(2):431–41. https://doi.org/10.1137/0111030.
30. Gear JI, Cox MG, Gustafsson J, Gleisner KS, Murray I, Glatting G, Konijnenberg M, Flux GD. EANM practical guidance on uncertainty analysis for molecular radiotherapy absorbed dose calculations. Eur J of Nucl Med Mol Imaging. 2018. https://doi.org/10.1007/s00259-018-4136-7.
31. Uribe CF, Esquinas PL, Tanguay J, Gonzalez M, Gaudin E, Beauregard J-M, Celler A. Accuracy of 177Lu activity quantification in SPECT imaging: a phantom study. EJNMMI Phys. 2017;4(1):2. https://doi.org/10.1186/s40658-016-0170-3.

Publisher's Note